DNA Nanotechnology Hot Paper

How to cite: *Angew. Chem. Int. Ed.* **2021**, *60*, 23241 – 23247
International Edition: doi.org/10.1002/anie.202107829
German Edition: doi.org/10.1002/ange.202107829

Programmable Site-Specific Functionalization of DNA Origami with Polynucleotide Brushes

Yunqi Yang[+], Qinyi Lu[+], Chao-Min Huang, Hongji Qian, Yunlong Zhang, Sonal Deshpande, Gaurav Arya, Yonggang Ke,* and Stefan Zauscher**

Abstract: *Combining surface-initiated, TdT (terminal deoxynucleotidyl transferase) catalyzed enzymatic polymerization (SI-TcEP) with precisely engineered DNA origami nanostructures (DONs) presents an innovative pathway for the generation of stable, polynucleotide brush-functionalized DNA nanostructures. We demonstrate that SI-TcEP can site-specifically pattern DONs with brushes containing both natural and non-natural nucleotides. The brush functionalization can be precisely controlled in terms of the location of initiation sites on the origami core and the brush height and composition. Coarse-grained simulations predict the conformation of the brush-functionalized DONs that agree well with the experimentally observed morphologies. We find that polynucleotide brush-functionalization increases the nuclease resistance of DONs significantly, and that this stability can be spatially programmed through the site-specific growth of polynucleotide brushes. The ability to site-specifically decorate DONs with brushes of natural and non-natural nucleotides provides access to a large range of functionalized DON architectures that would allow for further supramolecular assembly, and for potential applications in smart nanoscale delivery systems.*

Introduction

Over the last two decades, research in DNA nanotechnology has seen astonishing growth and has yielded exquisite DNA-based nanostructures that span a broad range of sizes and complexity.[1] DNA origami nanostructures (DONs) have been widely investigated for biomedical applications, such as biosensing,[2] in vivo imaging,[3] and drug and gene delivery,[4] due to their inherent biocompatibility, exquisite control over nanoscale geometry, mechanical properties, and suitability for site-specific functionalization.[5] However, the utility of DONs in biological environments is often compromised by their instability under denaturation conditions and damage by nuclease digestion.[6] These are particularly important factors that need to be considered for drug delivery applications where DONs have been investigated as nanoparticle-based delivery platforms to overcome the drawbacks of traditional small-molecule therapeutics (e.g., poor solubility, quick excretion by the renal system, and biodegradation).[7]

A strategy to mitigate instability issues is to "coat" DONs with functional groups that shield the origami core from the biological environment. To this end, a variety of approaches have been developed to cover DONs with lipid bilayers,[8] proteins,[9] peptides,[10] polymers,[11] and peptoids.[12] In most of these approaches, the adsorption of the protecting moieties is driven by hydrophobicity or electrostatic interactions between positively charged molecules and negatively charged DONs. While these protection methods improve the overall stability of DONs under specific conditions, the non-covalent binding between the protecting moieties and the DON surface can still be easily disrupted by mechanical forces and changes in the surrounding environment. Moreover, current methods are unable to produce tunable and site-specific functionalization of DONs with (bio)polymeric brush layers, which is crucial for taking full advantage of the inherent programmability of DONs for biomedical and other emerging applications. To the best of our knowledge, only a few studies have so far reported the in situ formation of nanopatterned synthetic polymers on the surface of DNA origami. For example, Tokura et al. have achieved this by atom-transfer radical polymerization, though the average height of these polymers was only ≈ 1 nm, which is insufficient for the protection of the DNA origami cores.[13] Earlier, Sørensen et al. reported the formation of nanopatterned DNA origami structures using macromolecule-modified strands as staples.[17] The large macromolecules were first conjugated to dNTPs by click chemistry and the reaction product was then attached to staple strands using TdT. Nevertheless, this method allows the incorporation of only a handful of macromolecule-modified dNTPs due to the limited ability of TdT to incorporate large non-natural nucleotides. In addition, there might be potential difficulty in assembly of origami using a large number of staple strands

[*] Y. Yang,[+] Dr. C. Huang, Prof. Dr. G. Arya, Prof. Dr. S. Zauscher
Department of Mechanical Engineering and Materials Science, Duke University, Durham, NC 27708 (USA)
E-mail: gaurav.arya@duke.edu
zauscher@duke.edu
Prof. Dr. Y. Ke
Department of Biomedical Engineering, Georgia Institute of Technology and Emory University, Atlanta, GA 30322 (USA)
E-mail: yonggang.ke@emory.edu
Q. Lu,[+] Y. Zhang
Department of Chemistry, Emory University
Atlanta, GA 30322 (USA)
H. Qian, Dr. S. Deshpande
Department of Biomedical Engineering, Duke University
Durham, NC 27708 (USA)
[+] These authors contributed equally to this work.
Supporting information and the ORCID identification number(s) for the author(s) of this article can be found under: https://doi.org/10.1002/anie.202107829.

having macromolecule modifications, which also limits the density of surface modification using this method.

Recently, we developed a new biomimetic method—TdT (terminal deoxynucleotidyl transferase) catalyzed enzymatic polymerization (TcEP)—to synthesize high molecular weight (MW), single-stranded DNA (ssDNA) homo- and block-co-polynucleotides with low polydispersity.[14] TcEP uses the template-independent polymerase TdT to sequentially add 3′-deoxyribonucleoside 5′-triphosphates (dNTPs) to an oligonucleotide primer.[15] We showed that TdT can polymerize both natural and non-natural nucleotides into single-stranded DNA (ssDNA),[16] which enables the introduction of various functionalities into polynucleotide chains, including clickable groups, fluorescent dyes, hydrophobic groups, and cytotoxic moieties.

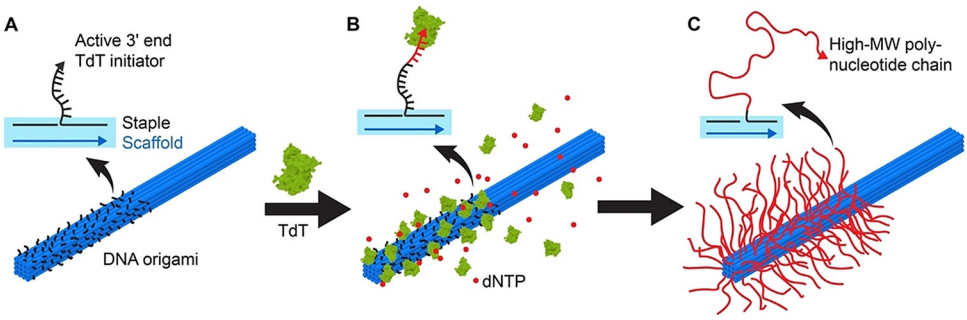

Figure 1. Schematic showing the programmable initiation of polynucleotide brush growth by surface-initiated TdT-catalyzed enzymatic polymerization (SI-TcEP). A) DNA origami partially modified with 3′ oligo(dT) initiators on the surface. B) Polynucleotide brush growth by SI-TcEP using TdT. C) DNA origami site-specifically modified with polynucleotide brushes on the surface after SI-TcEP reaction.

Here, we report on the design, synthesis, and characterization of stable and adaptive polynucleotide-functionalized DNA origami nanostructures (pn-DONs) through the synergistic combination of surface-initiated polynucleotide brush synthesis using TcEP with precisely engineered DNA origami.[18] Importantly, we show that these structures can be readily designed using existing origami design tools and their morphologies accurately predicted using coarse-grained molecular dynamics simulations. Our experimental results show that we have precise control over not only the shape of the origami core, but also the location, height, and functional composition (natural vs. non-natural nucleotides) of the polynucleotide brush. Furthermore, we show that pn-DONs have significantly higher nuclease resistance compared to unprotected DNA origami, and that this stability can be spatially programmed by site-specific design of the TcEP initiation sites on the surface of DONs. The resulting adaptive pn-DON degradation could be harnessed for DNA-based drug delivery vehicles to facilitate cellular uptake. Compared to a recent publication which reported the modification of DNA origami with polydopamine brushes of ≈10 nm height via photocontrolled polymerization,[19] we were able to produce modified DNA origami with polynucleotide brushes of heights in excess of 100 nm. Furthermore, our method allows the modification of DNA origami with polynucleotide brushes containing a range of functional groups, which enables sequential modification with desired molecules, further expanding the application of this system.

Results and Discussion

Our approach for creating pn-DONs is summarized in Figure 1. From the vast array of possible 3D DNA nanostructures, we choose rod-shaped 16-helix bundle (16HB) and 6-helix bundle (6HB) origami because of their simple geometry and the ease with which their lengths and widths can be tuned (Figures 1 A and S1–S4). The DNA nanorods were assembled by mixing and annealing the scaffold DNA strands with staple DNA strands in buffer solutions (see Methods). A 16HB origami nanorod (140 nm long, 10 nm wide, square cross-section) has 144 evenly distributed staple 3′ ends on its surface, whereas a 6HB origami nanorod (400 nm long, 6 nm wide, hexagon cross-section) has 162 staple 3′ ends on its surface (Figure S2). By using selected staple strands with 3′-oligo(dT) overhangs, TdT catalyzed enzymatic polymerization can be programmed to site-specifically initiate ssDNA brush growth on the surface of DNA origami nanorods (Figures 1 B and S2). Since the monomer to initiator (M/I) concentration ratio determines the degree of polymerization,[14b] we are able to synthesize a uniform polynucleotide brush layer onto the 3′-overhang-modified regions of the nanorods (Figure 1 C). For brevity, we term the oligo(dT) modified DONs as 16HB-S^{a}_{b} or 6HB-S^{a}_{b}, where *a* specifies the number of modified surfaces and *b* specifies the fraction of a surface that is modified. Furthermore, we term the polynucleotide brush-functionalized DONs as 16HB-S^{a}_{b}-pn_{c} or 6HB-S^{a}_{b}-pn_{c}, where *c* reflects the expected number of bases in the poly(dT) brush.

For a typical SI-TcEP reaction, we mixed DONs, dTTP, and TdT together in the TdT reaction buffer and incubated the mixture at 37 °C overnight. The resulting pn-DONs were purified by centrifugal filtration and characterized by agarose gel electrophoresis, and, after deposition onto a mica surface, by tapping mode atomic force microscopy (AFM) in air. To control the molecular weight (height) of the DNA brushes, we systematically varied the feed ratio (M/I) of monomer (i.e., dTTP) to initiator (i.e., oligo(dT) extensions on the surface of DONs) on the fully decorated 16HB (16HB-$S^{4}_{1/1}$).[14b] Gel electrophoresis showed that the degree of polymerization increased with increasing M/I (Figures 2 A and S5A). AFM imaging showed that fully decorated DONs were covered with a dense polynucleotide brush corona (Figures 2 B and S6). The brush height estimated from AFM image analysis increased almost linearly with M/I ratio, i.e., brush MW (Figure S5B). We also studied the effect of SI-TcEP reaction time (2 h, 6 h, 24 h) on polynucleotide brush growth at a constant M/I = 500. Our results suggest that the surface-

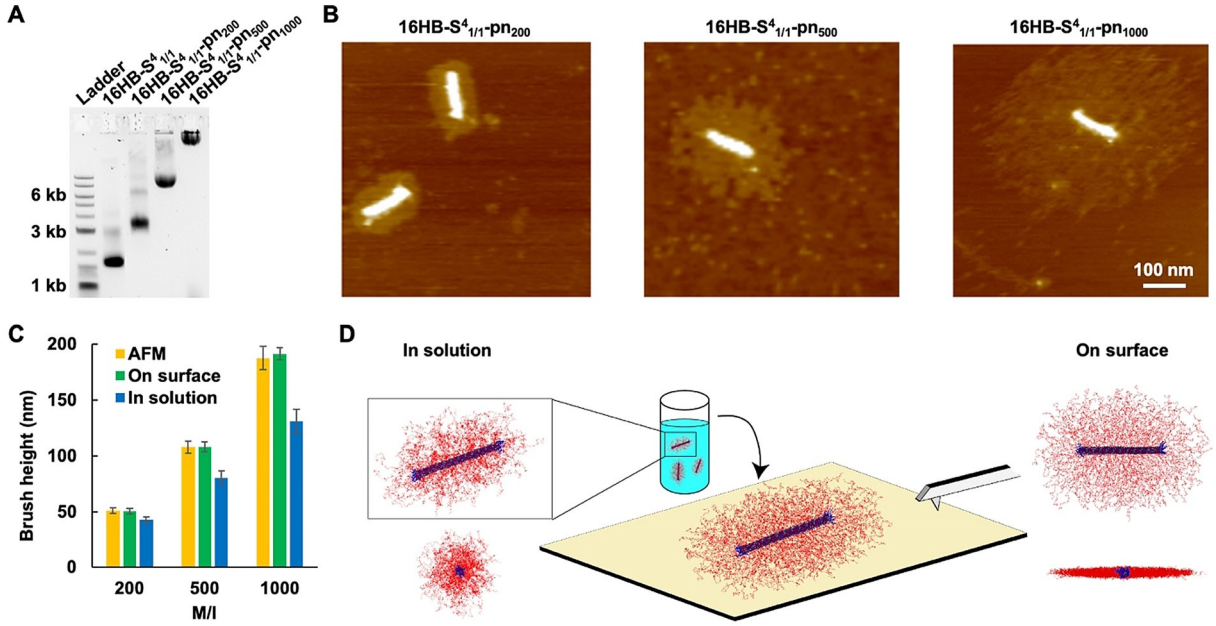

Figure 2. Formation of 16HB pn-DONs with controllable brush height. A) Agarose gel image and B) AFM images showing the controllable length of poly(dT) corona on 16HB-$S^4_{1/1}$ with different feed ratios (M/I = 200, 500, and 1000). C) Bar graph comparing the brush heights of 16HB-$S^4_{1/1}$-pn_{200}, 16HB-$S^4_{1/1}$-pn_{500}, and 16HB-$S^4_{1/1}$-pn_{1000} obtained from AFM image analysis with those predicted by 2D (on surface) and 3D (in solution) oxDNA simulations (see Table S1 for more details). D) Simulation results of 16HB-$S^4_{1/1}$-pn_{500} (top and side view) showing the morphology difference between structures in solution and on surface.

initiated polymerization reaction is fast, approaching completion already after 2 hours (Figure S7).

To elucidate details of the polynucleotide brush conformation on the surface of DONs we carried out oxDNA coarse-grained molecular dynamics simulations[20] of the structures in solution and after deposition onto a surface (Figures 2 D, S8–S12). The simulations reveal that pn-DONs are stable over the entire time of the simulation (> 150 μs), and that the polynucleotide chains adopt a moderately stretched conformation in solution, likely due to their relatively high surface grafting density (distance between chain initiation sites ≪ chain size) and weak electrostatic repulsion between their negatively charged backbones. The brush segment density plotted as a function of distance r from the origami surface suggests that the chains exhibit classic cylindrical brush behavior, with the segment density decaying as $\approx r^{-0.65}$ (Figure S10).[21] Chain stretching increases when the structures are confined in 2D to mimic the surface-adsorbed state visualized by AFM (Figure S11). The predicted brush heights of the surface-confined structures agree remarkably well with those obtained from analyses of AFM images (compare yellow and green bars in Figure 2 C, and values in Table S1). This agreement suggests that the predicted brush heights in solution (blue bars in Figure 2 C) should then likely provide a reasonable estimate of the "true" height of the brush on the origami surface. Furthermore, simulations show that lowering the ionic strength ($[Na^+]$) leads to a slight increase in the average brush height due to reduced charge screening (Figure S12).

We show next that site-specific polynucleotide brush growth can be achieved by designing DONs with oligo initiator extensions only at specific locations on the surface. The gel image in Figure 3 A shows the change in MW after SI-TcEP of three DONs with different patterns of initiation sites (16HB-$S^1_{1/1}$, 16HB-$S^4_{1/2}$, and 16HB-$S^4_{1/1}$). Before SI-TcEP, the mobility of DONs on the gel is quite similar, likely because

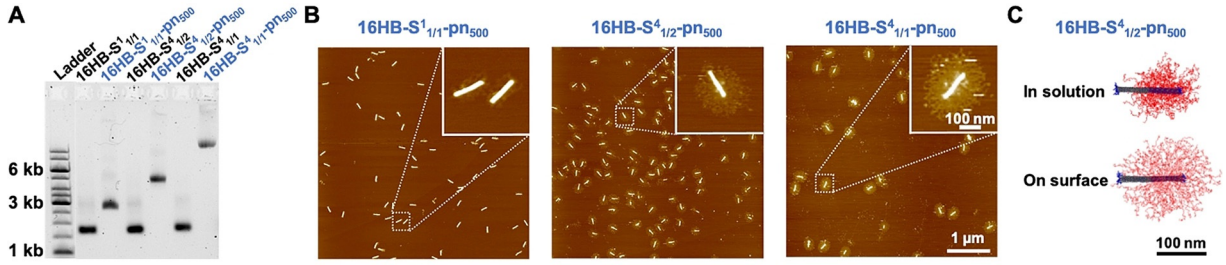

Figure 3. Site-specific modification of 16HBs with polynucleotide brushes. A) Agarose gel electrophoresis image and B) AFM images showing site-specific initiation of polynucleotide brush growth (M/I = 500) on 16HB. 16HB-$S^1_{1/1}$: 16HB with full-decorated poly(dT) extensions on 1 side (36 extensions); 16HB-$S^4_{1/2}$: 16HB with half-decorated poly(dT) extensions on all 4 sides (72 extensions); 16HB-$S^4_{1/1}$: 16HB with full-decorated poly(dT) extensions on all 4 sides (144 extensions). C) oxDNA simulations of 16HB-$S^4_{1/2}$-pn_{500} in solution and on surface.

the MW differences due to the different number of oligo(dT) extensions (8 nt) on the DON surfaces are small. After SI-TcEP (M/I = 500), however, the resulting pn-DONs have distinctly different MWs due to the different number of poly(dT) chains emanating from the surfaces. For example, for the 16HB-$S^{1}_{1/1}$-pn_{500}, the poly(dT) brushes exist only on one DON surface (Figure S2A). However, due to the random orientation of pn-DONs on the mica surface during drop casting, the AFM image is unable to properly show this single surface modification effect clearly (Figure 3B). Nevertheless, compared to the 16HB-$S^{4}_{1/1}$-pn_{500}, the brush density on 16HB-$S^{1}_{1/1}$-pn_{500} is visibly much lower. The AFM image of the half-decorated DONs (16HB-$S^{4}_{1/2}$-pn_{500}) shows brushes emanating from one half of the length of the origami core and extending to the other, undecorated half (Figure 3B). We attribute this effect to the flattening and spreading of the polynucleotide chains on the mica surface after drop-casting and drying. This behavior is also predicted by our simulations of pn-DONs on surface (Figure 3C). Additional demonstrations of spatial programmability using 16HB-$S^{4}_{1/3}$ and 16HB-$S^{4}_{1/6}$ systems are shown in Figure S13.

We verified the spatial programmability of brush growth using an entirely different DON core design, i.e., the 6HB, which is much longer and thinner compared to the 16HB (Figures 4 and S2). We first designed and assembled 6HB origami with oligo(dT) initiation sites at different positions along the origami core (6HB-$S^{6}_{1/1}$, 6HB-$S^{6}_{13/27}$, 6HB-$S^{6}_{5/27+5/27}$, and 6HB-$S^{6}_{7/27}$), and then subjected the resulting DONs to SI-TcEP (M/I ratio = 500). Figure 4B shows excellent agreement between the pn-DON conformations predicted by our simulations and those observed in AFM images. Because 6HBs are significantly longer than 16HBs, one can distinguish pn-DONs with poly(dT) brush corona at different positions on 6HBs more clearly.

It is known that a dense oligonucleotide brush layer is more resistant to nuclease degradation.[22] This also holds true

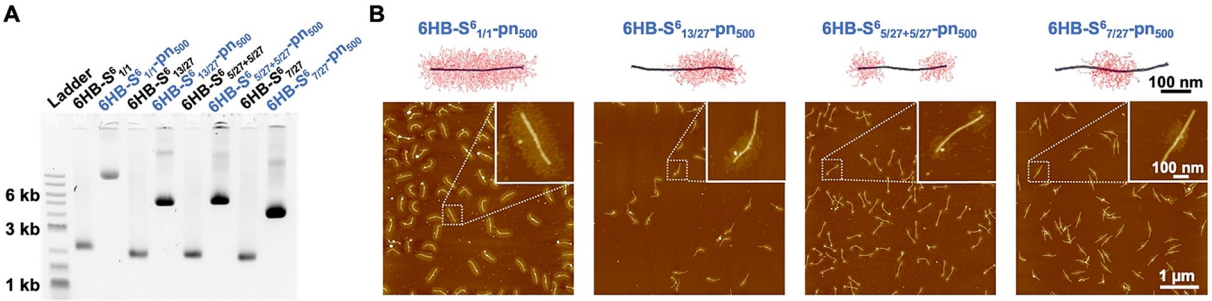

Figure 4. Site-specific modification of 6HBs with polynucleotide brushes. A) Agarose gel electrophoresis image and B) 2D (on surface) simulation results and AFM images showing site-specific initiation of polynucleotide brush growth (M/I = 500) on 6HB. 6HB-$S^{6}_{1/1}$: 6HB with full-decorated poly(dT) extensions (162 extensions); 6HB-$S^{6}_{13/27}$: 6HB with half-decorated poly(dT) extensions on one end (78 extensions); 6HB-S^{6}5/27 + 5/27: 6HB with partial poly(dT) extensions on both ends (60 extensions); 6HB-$S^{6}_{7/27}$: 6HB with partial poly(dT) extensions in the middle (42 extensions).

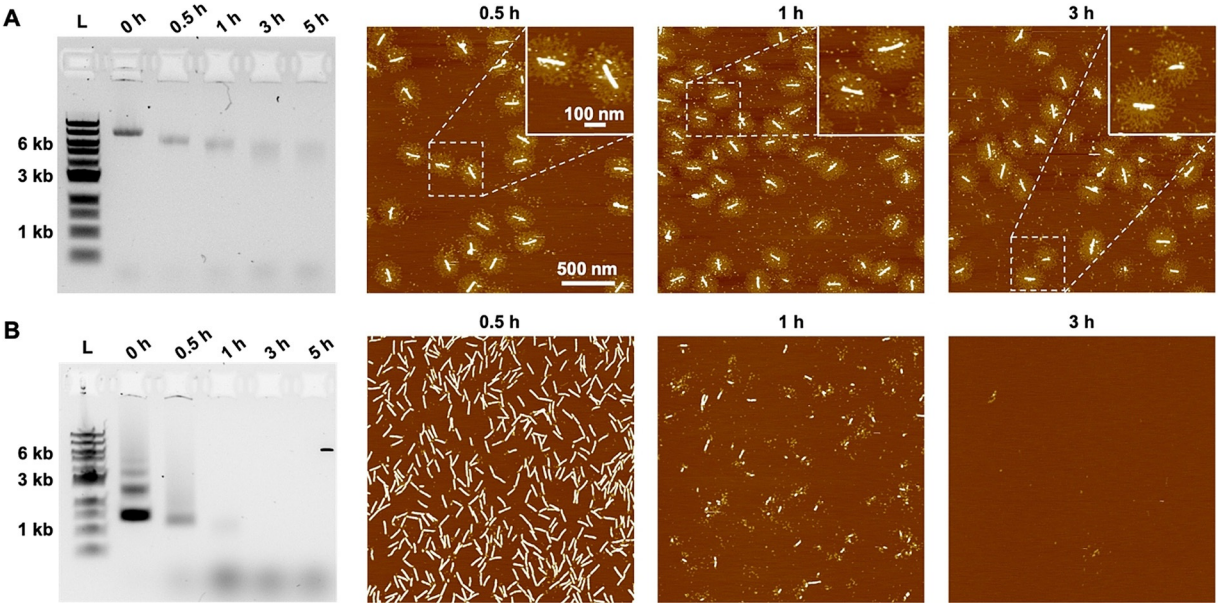

Figure 5. Nuclease stability of 16HB DONs with and without polynucleotide brushes. Agarose gel electrophoresis image and AFM images showing the stability of DNA origami A) with (16HB-$S^{4}_{1/1}$-pn_{500}) and B) without (16HB-$S^{4}_{1/1}$) poly(dT) brush decoration after incubation with 3.6 U mL^{-1} DNase I for different lengths of time.

for pn-DONs, as shown by our results in Figure 5. Specifically, we compared the stability of 16HB and 16HB-$S^4_{1/1}$-pn_{500} when subjected to digestion by the endonuclease DNase I. The gel and AFM images both confirm that fully covered 16HB-$S^4_{1/1}$-pn_{500} pn-DONs are significantly more stable against degradation by DNase I at physiological concentration (3.6 U mL^{-1})[23] compared to the bare 16HBs at the same mass concentration (compare Figure 5A with 5B). We attribute the downward movement of bands for 16HB-$S^4_{1/1}$-pn_{500} to the partial degradation of the polynucleotide brushes, which protect the origami cores; furthermore, we attribute the background noise appearing in the AFM images of pn-DONs to residual TdT enzymes remaining in solution after TcEP reaction.

In addition to DNase I, we also investigated the stability of the brush-protected origami against 10% FBS (16HB-$S^4_{1/1}$-pn_{250} and 16HB-$S^4_{1/1}$-pn_{500}). Figure S14 shows that the brush height (i.e., M/I) affects the degradation kinetics substantially. While both pn-DONs show distinct bands in the gel even after 20 hours of incubation, degradation proceeds slower for the origami decorated with longer brushes, as seen by the higher intensity of bands for 16HB-$S^4_{1/1}$-pn_{500} in Figure S14C compared to the bands for 16HB-$S^4_{1/1}$-pn_{250} in Figure S14B. The upward movement of bands for pn-DONs after incubation with 10% FBS (Figure S14A) is likely due to the interaction of proteins in FBS with the pn-DONs, leading to a different mobility when subjected to an electric field. This behavior is different from that observed when incubated with DNase I (Figure 5A).

Lastly, we evaluated the stability of 6HB pn-DONs against DNase I degradation. The gel and AFM images showed that unlike the 16HB DONs and pn-DONs, the 6HB DONs and pn-DONs were almost completely degraded already after incubation for 1 h (Figure S15). These results are consistent with the lower grafting density of polynucleotide brushes on 6HB cores and the smaller width of 6HB cores compared to 16HB cores (Figures S2–S4). Nevertheless, AFM images show that brush-modified 6HB pn-DONs are still more stable than unmodified ones. This is consistent with the agarose gel image which shows a distinct band for pn-DONs even after 30 min, while DONs lacking a brush layer form a smear in the first 10 min (Figure S15).

Interestingly, the location for enzymatic attack on pn-DONs can be programmed by origami design. For example, after incubating the half-decorated 16HB (16HB-$S^4_{1/2}$-pn_{500}) with DNase I for 1 h, only the polynucleotide-covered segments of the origami core survive (Figures 6B, S16, and S17), as depicted schematically also in Figure 6A. By analyzing the areas of pn-DONs and the areas of their origami cores as a function of time from AFM images, we observed a peak shift in both cases, indicating that the brush corona acts as a sacrificial layer for the brush-protected segments of the origami core (Figures 6D, S16B, and S16C). Thus, by deliberately introducing TcEP initiation sites on DONs, we can a priori determine which segments of origami will be degraded. This is an important attribute of our structures that has implications for drug delivery through the design of cleavable DONs.[24]

This phenomenon of selective protection is more apparent in the context of longer 6HB origami. We incubated dumbbell-shaped 6HBs (6HB-$S^6_{5/27+5/27}$-pn_{500}) which were decorated with a poly(dT) brush corona at both ends of the nanorods with DNase I (0.5 U mL^{-1}). AFM images showed that the dumbbell-shaped pn-DONs were cleaved in the center region of the nanorod which has no poly(dT) brush modification, as indicated with arrows in Figure 6G. However, the resulting shorter segments of brush-modified origami survived for a significantly longer time in presence of DNase I. This is also apparent from the gel image (Figure 6F), which shows that in addition to the band at the higher MW position (corresponding to the original sample), another band at the lower MW position (corresponding to the protected segments of the origami core) appeared after 30 min, and thereafter only the band with the lower MW survived after 60 min.

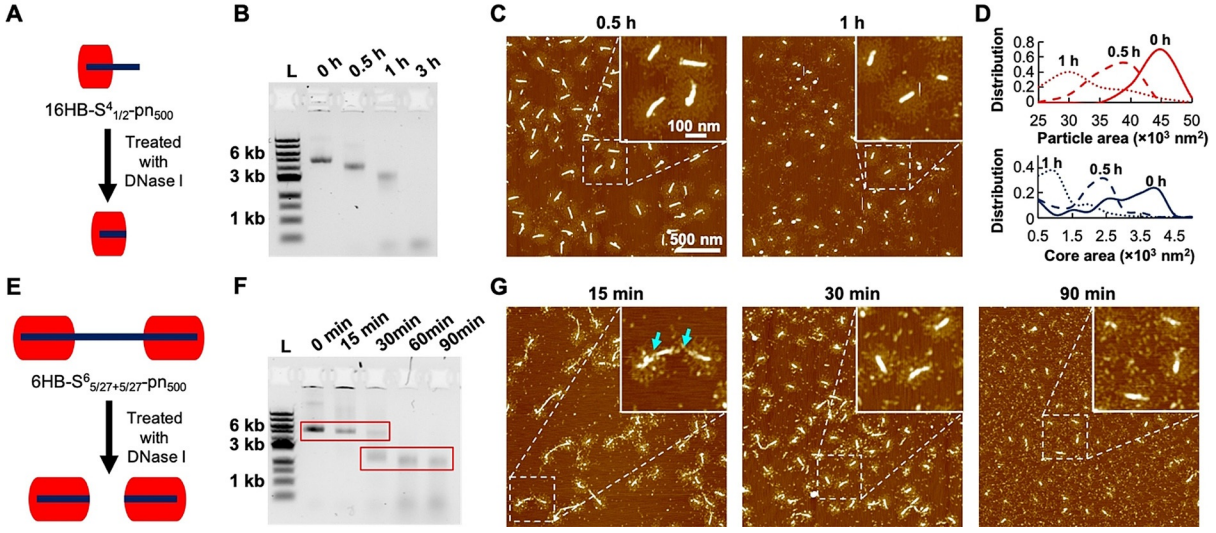

Figure 6. Controllable partial digestion of pn-DONs. A) Schematic, B) agarose gel electrophoresis image, C) AFM images, and D) size distribution of pn-DON particles and their origami cores showing the process of partial digestion of 16HB-$S^4_{1/2}$-pn_{500} by 3.6 U mL^{-1} DNase I. E) Schematic, F) agarose gel electrophoresis image, and G) AFM images showing the process of partial digestion of 6HB-$S^6_{5/27+5/27}$-pn_{500} by 0.5 U mL^{-1} DNase I.

Finally, we studied the stability of protected and unprotected origami in physiologically relevant buffer conditions. This is important because DONs are typically only stable at sufficiently high concentrations of divalent cations (e.g., 10 mM Mg^{2+} for 16HB and 6HB), which far exceed those in physiological conditions. AFM images showed that after incubating DONs (16HB) and pn-DONs (16HB-$S^4_{1/1}$-pn_{200} and 16HB-$S^4_{1/1}$-pn_{500}) in 1X DPBS with only 0.9 mM Ca^{2+} and 0.5 mM Mg^{2+} for 24 hours, both DONs and pn-DONs with short brushes (M/I = 200) disassembled (Figures S18D and S18E). However, pn-DONs with long polynucleotide brushes (M/I = 500) maintained their integrity even after 24 hours incubation (Figure S18F). This was corroborated by gel images of DONs and pn-DONs with shorter brushes (M/I = 200) (Figures S18A and S18B), which showed a larger extent of staple dissociation—as seen by the increase of band intensity at lower positions (< 500 bp)—than pn-DONs with longer brushes (Figure S18C). The observed upward shift in the bands for 16HB DON sample after incubation arises from the disassembly of origami, which results in increased size and thus slower migration in the agarose gel. On the other hand, the downward shift in the bands for both pn-DON samples (16HB-$S^4_{1/1}$-pn_{200} and 16HB-$S^4_{1/1}$-pn_{500}) suggests a loss of poly(dT) strands during disassembly, which leads to overall lower MW but still intact pn-DON structures that migrate faster in the agarose gel.

So far, as proof-of-concept, we have used natural nucleotide (dTTP) monomers for the polymerization reactions. However, as shown in Figure S19, we confirmed that TdT is able to polymerize 5-Fluoro-dUTP (5F-dUTP), a non-natural cytostatic nucleotide. This observation underscores the potential of pn-DONs for drug-delivery applications. Our approach can be applied even more broadly to also encompass chemically functionalized nucleotide analogues that could be harnessed for post-polymerization reactions, such as azide-alkyne cycloaddition "click" reactions. To this end, we showed that 5-Ethynyl-dUTP (5E-dUTP) can be polymerized by SI-TcEP (Figure S19). By introducing clickable groups into polynucleotide brushes, our approach can potentially be used for generating a broad range of site-specific chemical modifications on DNA origami, including incorporation of dyes, hydrophobic groups, and biotin molecules.

Conclusion

In summary, our research on the synergistic combination of surface initiated enzymatic polynucleotide brush synthesis with precisely engineered DNA origami is new and presents, guided by molecular simulations, an innovative pathway for the generation of tunable and stable polynucleotide brush-functionalized DNA nano- and meso-structures. Specifically, we have devised a strategy that harnesses the broad polymerization capability of TdT to synthesize DNA nanostructures by site-specifically programming the surface-initiated growth of polynucleotide brushes on the surface of DNA origami. We found that fully brush-decorated pn-DONs can be stable for many hours in presence of nucleases and physiologically relevant buffer conditions. We showed that site-specific, partial brush decoration will direct nuclease degradation primarily to unprotected areas of the origami core, thus providing a route to generate smart, cleavable pn-DONs. Finally, the ability of TdT to polymerize a broad range of nucleotide analogues enables the synthesis of polynucleotide brush-modified DNA origami which are poised to find applications ranging from drug delivery and biosensing to the generation of microreactors by supramolecular self-assembly.

Acknowledgements

S.Z. thanks the NIH for support through grant R21 EB026590-03. Y.K. and G.A. acknowledge the support of DOE grant DE-SC0020996, and NSF grants DMR-1654485 and ECCS-1807568. Computational resources were provided by the Duke Computing Cluster (DCC) and the Extreme Science and Engineering Discovery Environment (XSEDE) Program supported by NSF grant ACI-1053575.

Conflict of Interest

The authors declare no conflict of interest.

Keywords: DNA nanotechnology · drug delivery · molecular dynamics simulations · nuclease resistance · surface-initiated polymerization

[1] a) M. DeLuca, Z. Shi, C. E. Castro, G. Arya, *Nanoscale Horiz.* **2020**, *5*, 182 – 201; b) P. Wang, T. A. Meyer, V. Pan, P. K. Dutta, Y. Ke, *Chem* **2017**, *2*, 359 – 382; c) P. W. K. Rothemund, *Nature* **2006**, *440*, 297 – 302; d) F. Hong, F. Zhang, Y. Liu, H. Yan, *Chem. Rev.* **2017**, *117*, 12584 – 12640; e) T. Tørring, N. V. Voigt, J. Nangreave, H. Yan, K. V. Gothelf, *Chem. Soc. Rev.* **2011**, *40*, 5636 – 5646.

[2] A. H. Okholm, H. Aslan, F. Besenbacher, M. Dong, J. Kjems, *Nanoscale* **2015**, *7*, 10970 – 10973.

[3] a) R. Jungmann, M. S. Avendaño, J. B. Woehrstein, M. Dai, W. M. Shih, P. Yin, *Nat. Methods* **2014**, *11*, 313 – 318; b) M. Dai, R. Jungmann, P. Yin, *Nat. Nanotechnol.* **2016**, *11*, 798 – 807.

[4] a) J. Li, C. Fan, H. Pei, J. Shi, Q. Huang, *Adv. Mater.* **2013**, *25*, 4386 – 4396; b) P. D. Halley, C. R. Lucas, E. M. McWilliams, M. J. Webber, R. A. Patton, C. Kural, D. M. Lucas, J. C. Byrd, C. E. Castro, *Small* **2016**, *12*, 308 – 320; c) Y.-X. Zhao, A. Shaw, X. Zeng, E. Benson, A. M. Nyström, B. R. Högberg, *ACS Nano* **2012**, *6*, 8684 – 8691; d) Q. Zhang, Q. Jiang, N. Li, L. Dai, Q. Liu, L. Song, J. Wang, Y. Li, J. Tian, B. Ding, *ACS Nano* **2014**, *8*, 6633 – 6643.

[5] A. R. Chandrasekaran, N. Anderson, M. Kizer, K. Halvorsen, X. Wang, *ChemBioChem* **2016**, *17*, 1081 – 1089.

[6] Q. Jiang, S. Liu, J. Liu, Z. G. Wang, B. Ding, *Adv. Mater.* **2019**, *31*, 1804785.

[7] a) S. Senapati, A. K. Mahanta, S. Kumar, P. Maiti, *Signal Transduct. Target Ther.* **2018**, *3*, 7; b) A. Wicki, D. Witzigmann, V. Balasubramanian, J. Huwyler, *J. Controlled Release* **2015**, *200*, 138 – 157; c) S. Gupta, P. K. Gupta, G. Dharanivasan, R. S. Verma, *Nanomedicine* **2017**, *12*, 2675 – 2692.

[8] S. D. Perrault, W. M. Shih, *ACS Nano* **2014**, *8*, 5132 – 5140.

[9] J. Mikkilä, A. P. Eskelinen, E. H. Niemelä, V. Linko, M. J. Frilander, P. Törmä, M. A. Kostiainen, *Nano Lett.* **2014**, *14*, 2196 – 2200.

[10] N. Ponnuswamy, M. M. C. Bastings, B. Nathwani, J. H. Ryu, L. Y. T. Chou, M. Vinther, W. A. Li, F. M. Anastassacos, D. J. Mooney, W. M. Shih, *Nat. Commun.* **2017**, *8*, 15654.
[11] N. P. Agarwal, M. Matthies, F. N. Gür, K. Osada, T. L. Schmidt, *Angew. Chem. Int. Ed.* **2017**, *56*, 5460 – 5464; *Angew. Chem.* **2017**, *129*, 5552 – 5556.
[12] S. T. Wang, M. A. Gray, S. Xuan, Y. Lin, J. Byrnes, A. I. Nguyen, N. Todorova, M. M. Stevens, C. R. Bertozzi, R. N. Zuckermann, O. Gang, *Proc. Natl. Acad. Sci. USA* **2020**, *117*, 6339 – 6348.
[13] Y. Tokura, Y. Jiang, A. Welle, M. H. Stenzel, K. M. Krzemien, J. Michaelis, R. Berger, C. Barner-Kowollik, Y. Wu, T. Weil, *Angew. Chem. Int. Ed.* **2016**, *55*, 5692 – 5697; *Angew. Chem.* **2016**, *128*, 5786 – 5791.
[14] a) L. Tang, V. Tjong, N. Li, Y. G. Yingling, A. Chilkoti, S. Zauscher, *Adv. Mater.* **2014**, *26*, 3050 – 3054; b) L. Tang, L. A. Navarro, Jr., A. Chilkoti, S. Zauscher, *Angew. Chem. Int. Ed.* **2017**, *56*, 6778 – 6782; *Angew. Chem.* **2017**, *129*, 6882 – 6886.
[15] F. J. Bollum in *The Enzymes*, 3rd ed. (Ed.: P. D. Boyer), Academic Press, New York, **1974**, pp. 145 – 171.
[16] R. Gu, T. Oweida, Y. G. Yingling, A. Chilkoti, S. Zauscher, *Biomacromolecules* **2018**, *19*, 3525 – 3535.
[17] R. S. Sørensen, A. H. Okholm, D. Schaffert, A. L. B. Kodal, K. V. Gothelf, J. Kjems, *ACS Nano* **2013**, *7*, 8098 – 8104.
[18] a) D. C. Chow, W.-K. Lee, S. Zauscher, A. Chilkoti, *J. Am. Chem. Soc.* **2005**, *127*, 14122 – 14123; b) V. Tjong, L. Tang, S. Zauscher, A. Chilkoti, *Chem. Soc. Rev.* **2014**, *43*, 1612 – 1626; c) S. Deshpande, Y. Yang, A. Chilkoti, S. Zauscher in *Methods in enzymology*, *Vol. 627*, Elsevier, Amsterdam, **2019**, pp. 163 – 188.
[19] P. Winterwerber, S. Harvey, D. Y. W. Ng, T. Weil, *Angew. Chem. Int. Ed.* **2020**, *59*, 6144 – 6149; *Angew. Chem.* **2020**, *132*, 6200 – 6205.
[20] a) B. E. K. Snodin, F. Randisi, M. Mosayebi, P. Sulc, J. S. S. F. Romano, F. Romano, T. E. Ouldridge, R. Tsukanov, E. Nir, A. A. Louis, J. P. K. Doye, *J. Chem. Phys.* **2015**, *142*, 234901; b) J. P. K. Doye, T. E. Ouldridge, A. A. Louis, F. Romano, P. Sulc, C. Matek, B. E. K. Snodin, L. Rovigatti, J. S. Schreck, R. M. Harrison, W. P. J. Smith, *Phys. Chem. Chem. Phys.* **2013**, *15*, 20395 – 20414; c) L. Rovigatti, P. Šulc, I. Z. Reguly, F. Romano, *J. Comput. Chem.* **2015**, *36*, 1 – 8; d) S. Ze, C. E. Castro, G. Arya, *ACS Nano* **2017**, *11*, 4617 – 4630.
[21] a) J. Le Guillou, J. Zinn-Justin, *Phys. Rev. B* **1980**, *21*, 3976; b) K. Binder, A. Milchev, *J. Polym. Sci. Part B* **2012**, *50*, 1515 – 1555.
[22] D. S. Seferos, A. E. Prigodich, D. A. Giljohann, P. C. Patel, C. A. Mirkin, *Nano Lett.* **2009**, *9*, 308 – 311.
[23] E. Benson, A. Mohammed, J. Gardell, S. Masich, E. Czeizler, P. Orponen, B. Högberg, *Nature* **2015**, *523*, 441 – 444.
[24] L. Li, W. Sun, J. Zhong, Q. Yang, X. Zhu, Z. Zhou, Z. Zhang, Y. Huang, *Adv. Funct. Mater.* **2015**, *25*, 4101 – 4113.

Manuscript received: June 11, 2021
Accepted manuscript online: July 23, 2021
Version of record online: August 16, 2021

